Electronic supplementary information

Boosting CO_2 electroreduction over Co nanoparticles supported on N, B-co-doped graphitic carbon

Xinning Song,[a,b] *Weiwei Guo,*[a,b,c] *Xiaodong Ma,*[a,b] *Liang Xu,*[a] *Xingxing Tan,*[a,b] *Limin Wu,*[a,b] *Shunhan Jia,*[a,b] *Tianbin Wu,*[a] *Jun Ma,*[a] *Farao Zhang,*[d] *Jinchao Jia,*[d] *Xiaofu Sun**[a,b] *and Buxing Han**[a,b,e]

[a] *Beijing National Laboratory for Molecular Sciences, CAS Key Laboratory of Colloid and Interface and Thermodynamics, CAS Research/Education Center for Excellence in Molecular Sciences, Institute of Chemistry, Chinese Academy of Sciences, Beijing 100190, China.*

E-mail: sunxiaofu@iccas.ac.cn, hanbx@iccas.ac.cn

[b] *School of Chemical Sciences, University of Chinese Academy of Sciences, Beijing 100049, China*

[c] *College of Chemistry and Chemical Engineering, Qingdao University, Qingdao 266071, China*

[d] *Ningbo MaterChem Technology Co. Ltd., Ningbo 315830, China*

[e] *Shanghai Key Laboratory of Green Chemistry and Chemical Processes, School of Chemistry and Molecular Engineering, East China Normal University, Shanghai 200062, China*

Experimental Section

Experimental materials

Boric acid (99.5%) was provided by InnoChem Technology. 2-Methylimidazole (MIM, 99%) was provided by J&K Technology. Zinc nitrate hexahydrate ($Zn(NO_3)_2\cdot6H_2O$, >98%) and cobalt nitrate hexahydrate ($Co(NO_3)_2\cdot6H_2O$, 99 %) were supplied by Sinopharm Chemical Reagent. The ionic liquid, 1-butyl-3-methylimidazole hexafluorophosphate ($[Bmim]PF_6$, > 99%) was provided by the Green Chemistry and Catalysis Center, Lanzhou Institute of Chemical Physics, Chinese Academy of Sciences. Nafion N-117 proton exchange membrane (thickness 0.180 mm, exchange capacity $\geq$ 0.90 meg g^{-1}) and Toray carbon paper (CP, TGP-H-60, 19 × 19 cm^2) were obtained from Alfa Reagent. Polytetrafluoroethylene concentrated dispersion (PTFE, 60 wt % dispersion) was provided by Aladdin Reagent. Deionized water, methanol (analytical grade), ethanol (analytical grade), CO_2 (> 99.999%) were purchased from Beijing Analytical Instrument Factory.

Synthesis of precursors Co/Zn ZIFs

$Co(NO_3)_2\cdot6H_2O$ (0.273 g) and $Zn(NO_3)_2\cdot6H_2O$ (0.558 g) were first dissolved in 20 mL of methanol (solution A), and then 2-methylimidazole (0.616 g) was dissolved in 20 mL of methanol (solution B). The solution B was added dropwise to the solution A and the mixture was stirred at room temperature for 12 h. The suspension was separated by centrifugation at 6000 rpm for 5 min and washed three times with methanol to obtain the precipitate. Finally, the precipitate was dried overnight at 70 ^{o}C under vacuum to obtain Co/Zn ZIFs.

Synthesis of target catalytic materials

Co/Zn ZIFs and boric acid were ground and mixed well at the mass ratio of 5:1, 2:1 and 1:1, and the above precursors were kept at 800 ^{o}C for 1 h under Ar atmosphere (heating rate: 5 ^{o}C min^{-1}), then at 900 ^{o}C for 1 h, and then at 1000 ^{o}C for 1 h. After cooling to room temperature, Co-NB-1, Co-NB-2 and Co-NB-3 were obtained by artificial polishing for 20 min.

Synthesis of contrasting catalytic material

In order to reveal whether the boron element in Co-NB has any effect on the catalytic performance, a loaded cobalt catalyst (Co-N) was synthesized as a comparison material, and Co-N was prepared by the method described above for the synthesis of Co-NB, except that no boric acid was added.

Materials characterizations

X-ray diffraction (XRD) of the materials was measured on a Rigaku D/max-2500 diffractometer with an X-ray incident wavelength of 0.154 nm, a gas pedal voltage of 40 kV, and an acceleration current of 200 mA. Scanning electron microscope (SEM, HITACHI S-4800), Transmission Electron Microscope (TEM, JEOL-1011), and high-resolution transmission electron microscope (HRTEM, JEOL-2100F) were used to characterize the morphology of the materials. X-ray photoelectron spectroscopy (XPS) was performed by an X-ray photoelectron spectrometer Thermo Scientific ESCA Lab 250Xi using a 200 W Al Kα target with a basic pressure of about 3×10^{-10} mbar in the analysis chamber. The elemental content of cobalt was determined with an inductively coupled plasma emission spectrometer (VISTA-MPX). The elemental content of carbon, nitrogen and boron was determined with an elemental analyzer (Flash EA1112). The specific surface area and pore properties of the materials were determined by Micromeritics ASAP 2020 sorptometer with Brunauer-Emmett-Teller (BET) method. X-ray absorption spectroscopy (XAS) was performed at the 1W1B experimental station of Beijing Synchrotron Radiation Center (BSRF), and the data were processed using Athena and Artemis software.

Electrode preparation

A mixture of cobalt-based catalyst (1.0 mg), 6 wt% PTFE dispersion and 100 μL acetone was sonicated for 10 min to form a homogeneous ink. 100 μL of the ink was quantitatively pipetted with a pipette gun and dropped onto a 0.5×1 cm^2 surface of carbon paper and blown dry with N_2 to obtain a working electrode.

Electrocatalytic CO_2 reduction

The electrocatalytic reduction of CO_2 was tested in an H-type electrochemical cell in a three-electrode system. The counter electrode was Pt net and the reference electrode was Ag/Ag^+. The working and reference electrodes were placed in the cathode chamber and the counter electrode was placed in the anode chamber. In the experiments, the cathode and anode compartments were separated through a Nafion 117 proton exchange membrane. H_2SO_4 aqueous solution (0.5 M) was used as anodic electrolyte. H^+ can be transferred from anode compartment to cathode compartment through Nafion 117 proton exchange membrane, which is the proton source. Before the test, CO_2 was passed through the electrolyte for at least 30 min to form a saturated solution of CO_2. Linear scanning voltammetry (LSV) curves were measured in the CO_2-saturated electrolyte, acetonitrile solution containing 0.5M 1-butyl-3-methylimidazolium hexafluorophosphate ([Bmim]PF_6), with a potential range of 0 V to -2.4 V and a scan rate of 20 mV/s.

Product analysis

The gaseous products were collected in gas bags and analyzed by gas chromatography (GC, HP 4890D) for the composition of the gaseous products and the liquid products were detected by nuclear magnetic resonance (^{1}H-NMR, BrukerAvance III 400 HD).

Calculation of the Faraday efficiency of products.

Since the products are mainly CO and H_2, only the Faraday efficiencies of the gaseous products needed to be calculated. The volume % of CO and H_2 could be obtained from the GC peak areas and calibration curve of the TCD detector. Since the CO_2 flow rate was constant, the moles of CO and H_2 per second could be calculated. The theoretical moles of CO and H_2 per second could be obtained from the current density. Therefore, the Faraday efficiency was:

FE = moles of product per second/theoretical moles of equivalent per second

Calculation of TOF.

The TOF for CO was calculated as follows, and the method is the same as the literature^{S1}:

$$TOF = \frac{I_{CO}/nF}{m_{cat} \times \omega \times \alpha / M_{Co}} \times 3600$$

TOF: turnover frequency, h^{-1}.

I_{CO}: partial current for certain product, A.

n: the number of electrons transferred for product formation, which is 2 for CO

F: Faradaic constant, 96485 C mol^{-1}.

m$_{cat}$: catalyst mass in the electrode, g.

α: the ratio of active atoms in Co NPs (estimated as the ratio of surface area to volume)

ω: Co loading in the catalyst.

M$_{Co}$: atomic mass of Co, 58.93 g·mol^{-1}.

TOF of Co-NB-2 at -2.4 V:

$I_{CO} = 18.4\ mA$; $m_{cat} = 1.0\ mg$; $\omega = 11.86\%$; $r = 12.5\ nm$; $\alpha = \frac{4\pi r^2}{4\pi r^3/3} = 0.24$;

$$TOF = \frac{I_{CO}/nF}{m_{cat} \times \omega \times \alpha / M_{Co}} \times 3600 = 40.93\ h^{-1}$$

Quasi-operando X-ray photoelectron spectroscopy

To study the valence state of cobalt during the reaction, quasi-operando XPS measurements of the four catalysts were carried out in a glove box after 30 min of the reaction. The reacted electrode materials were immersed in acetone solution and then immediately placed in the glove box. The electrode materials were blown dry with an earwash ball, cut to 2 × 2 mm and glued onto the holder. The holder was evacuated to prevent oxidation of the material. The subsequent procedure was the same as conventional XPS.

Tafel analysis

The partial current density of CO was measured at different potentials and the equilibrium potential was known by extrapolation. The overpotential was obtained from the difference between the equilibrium potential and the applied potential. Repeated electrolysis experiments were performed at each potential to obtain data on the overpotential and partial current density of CO in the H-type electrolytic cell. Finally, the Tafel plots were plotted.

Electrochemical surface areas (ECSAs) study

The electrochemical surface area was proportional to the C$_{dl}$ value. Cyclic voltammetry was performed in MeCN containing 0.5 M [Bmim]PF$_6$ solution using a three-electrode system at 25 °C. Cyclic voltammograms were measured at six different scan rates of

20, 30, 50, 80, 100, and 120 mV s^{-1} at -1.60 to -1.70 V vs Ag/Ag^+ for the catalysts, and the double layer capacitance (C_{dl}) of the catalysts were obtained. C_{dl} was estimated by plotting Δj (j_a-j_c) at -1.65 V vs Ag/Ag^+ versus the scan rate, where j_a and j_c were the anode and cathode current densities, respectively. The linear slope was equivalent to twice the C_{dl}.

Electrochemical impedance spectroscopy (EIS) study

EIS measurements were performed in 0.5 M $[Bmim]PF_6$-MeCN at open circuit potential (OCP) with an amplitude of 5 mV of 10^{-1} to 10^6 Hz.

Supplementary Figures

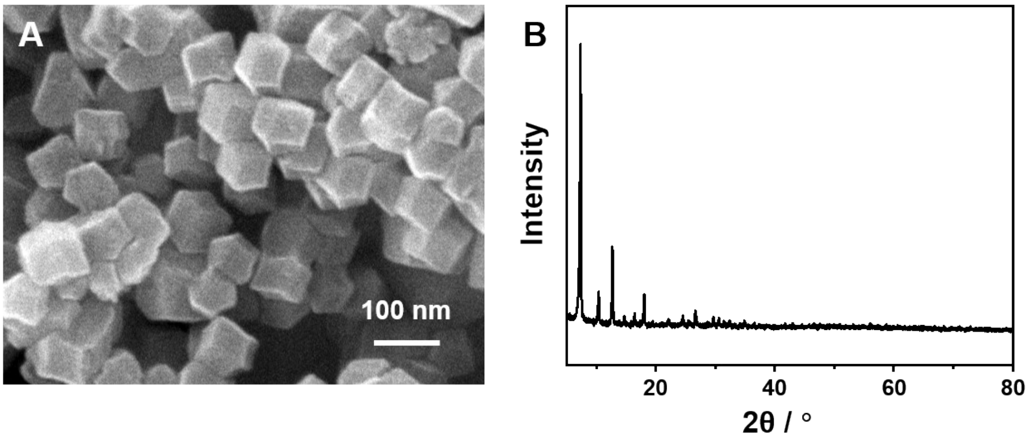

Fig. S1 A) SEM image and B) XRD pattern of ZIF-8.

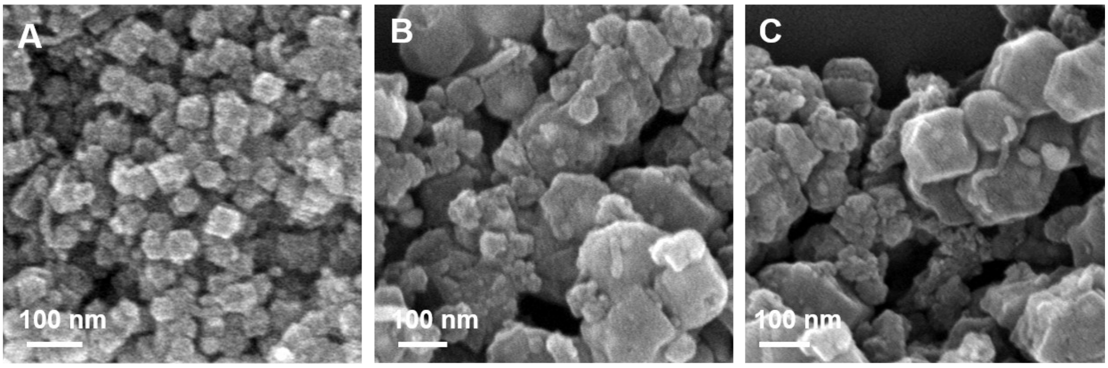

Fig. S2 SEM images of A) Co-N, B) Co-NB-1 and C) Co-NB-3.

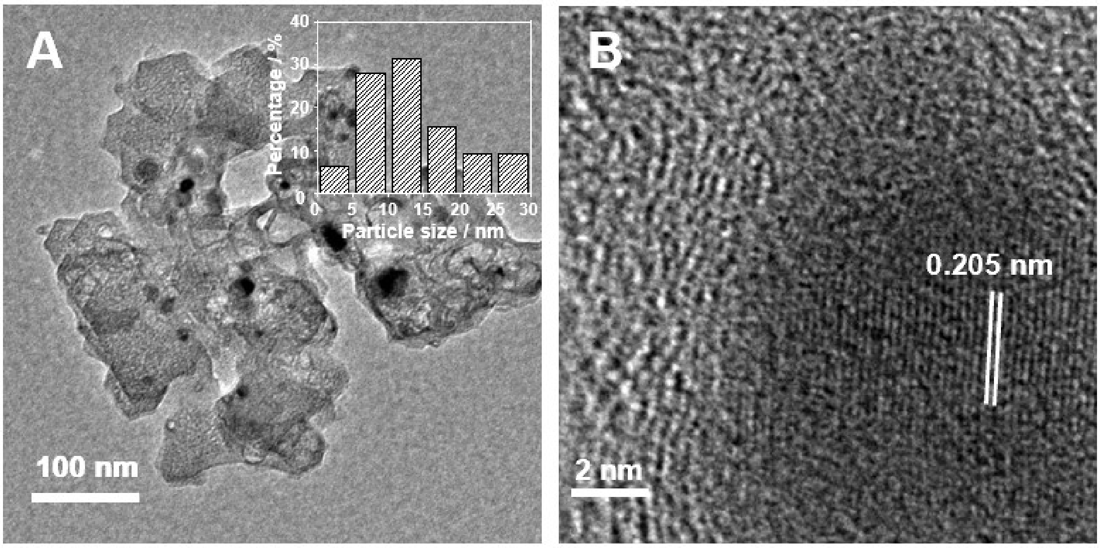

Fig. S3 A) TEM image and particle size distribution and B) HR-TEM image of Co-N.

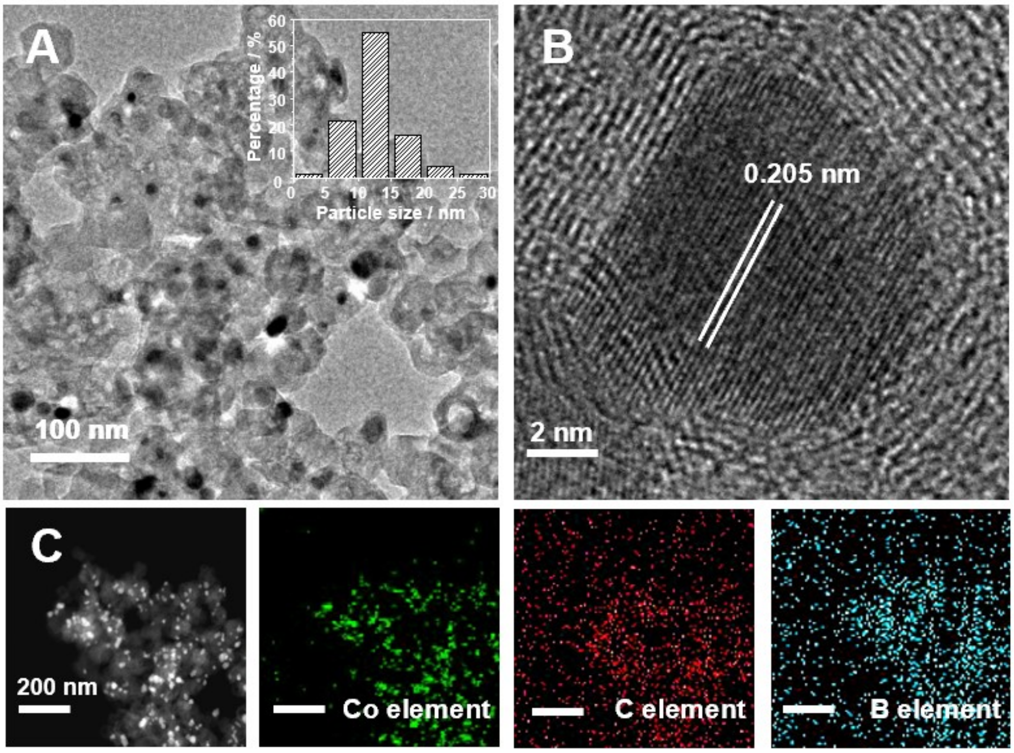

Fig. S4 A) TEM image and particle size distribution, B) HR-TEM image and C) Elemental mappings images of Co-NB-1.

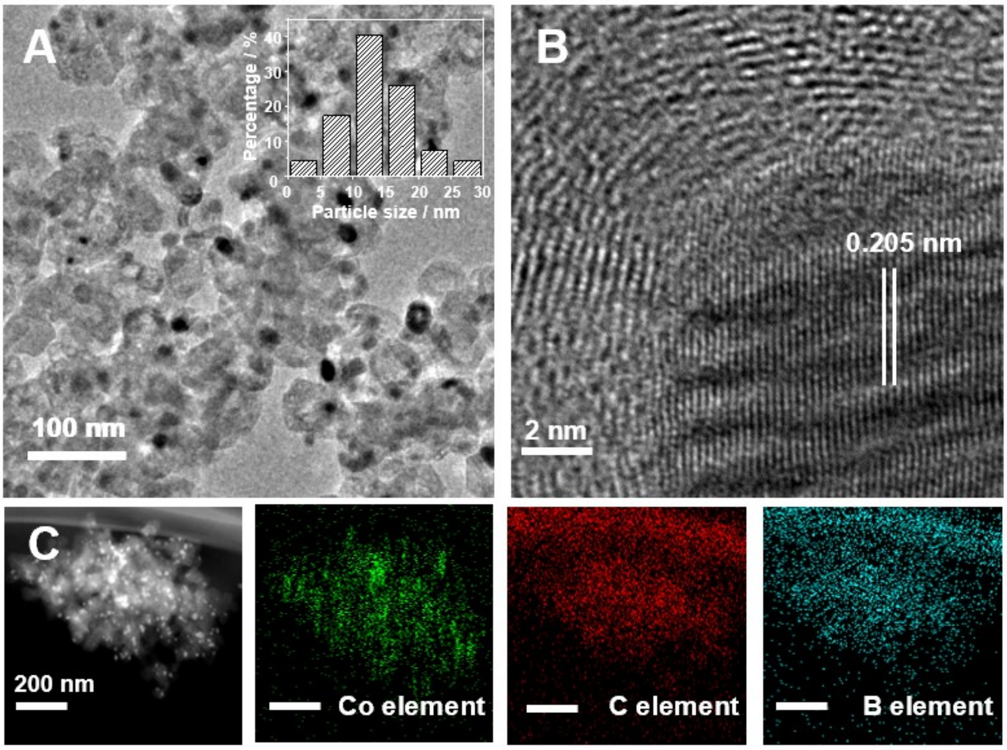

Fig. S5 A) TEM image and particle size distribution, B) HR-TEM image and C) Elemental mappings images of Co-NB-3.

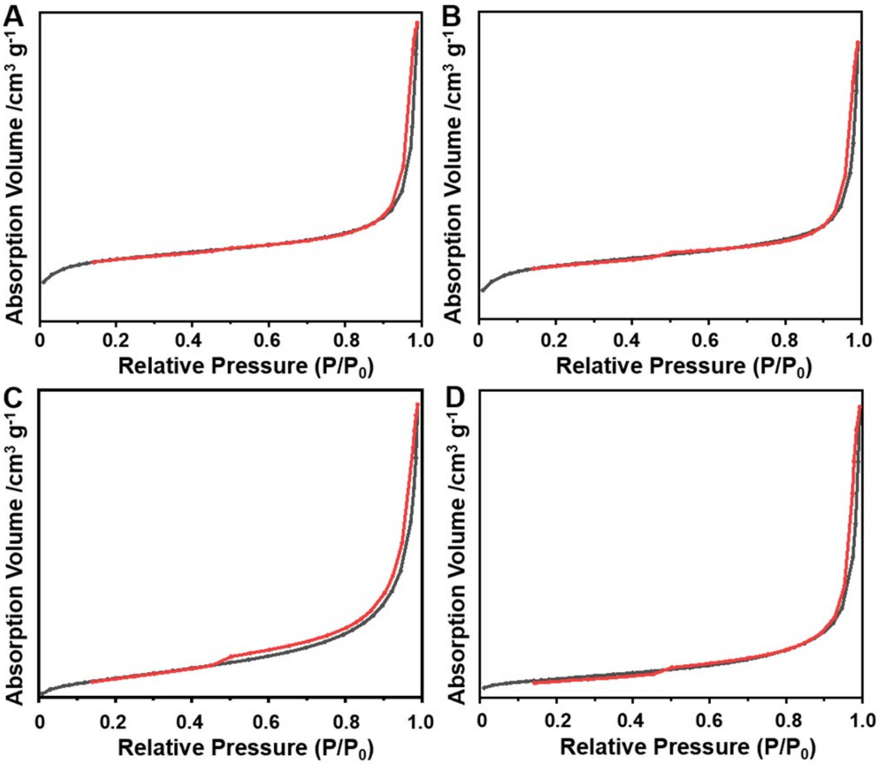

Fig. S6 N_2 adsorption/desorption isotherms of A) Co-N, B) Co-NB-1, C) Co-NB-2, D) Co-NB-3.

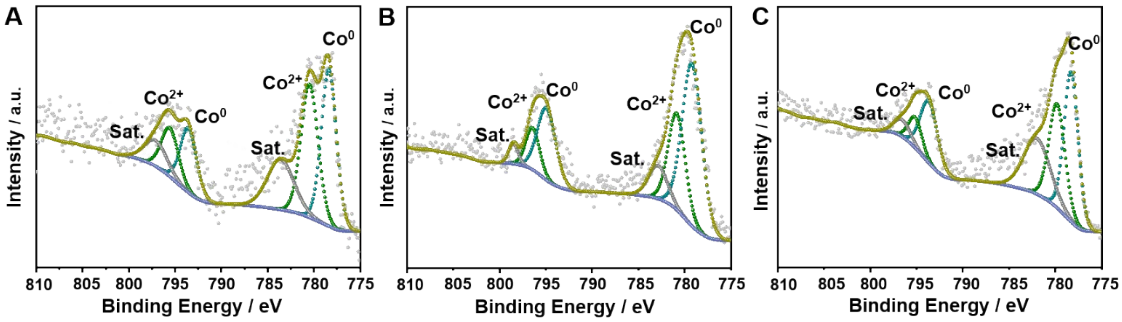

Fig. S7 XPS spectra of Co 2p orbits for A) Co-N, B) Co-NB-1, C) Co-NB-3.

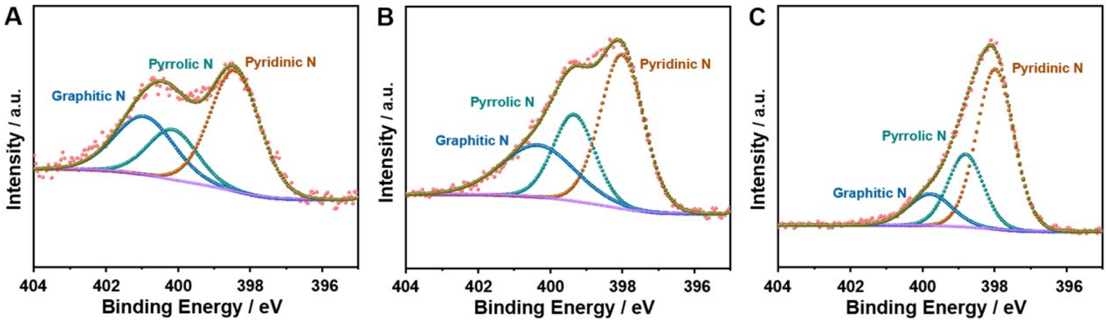

Fig. S8 XPS spectra of N1s orbits for A) Co-N, B) Co-NB-1 and C) Co-NB-3.

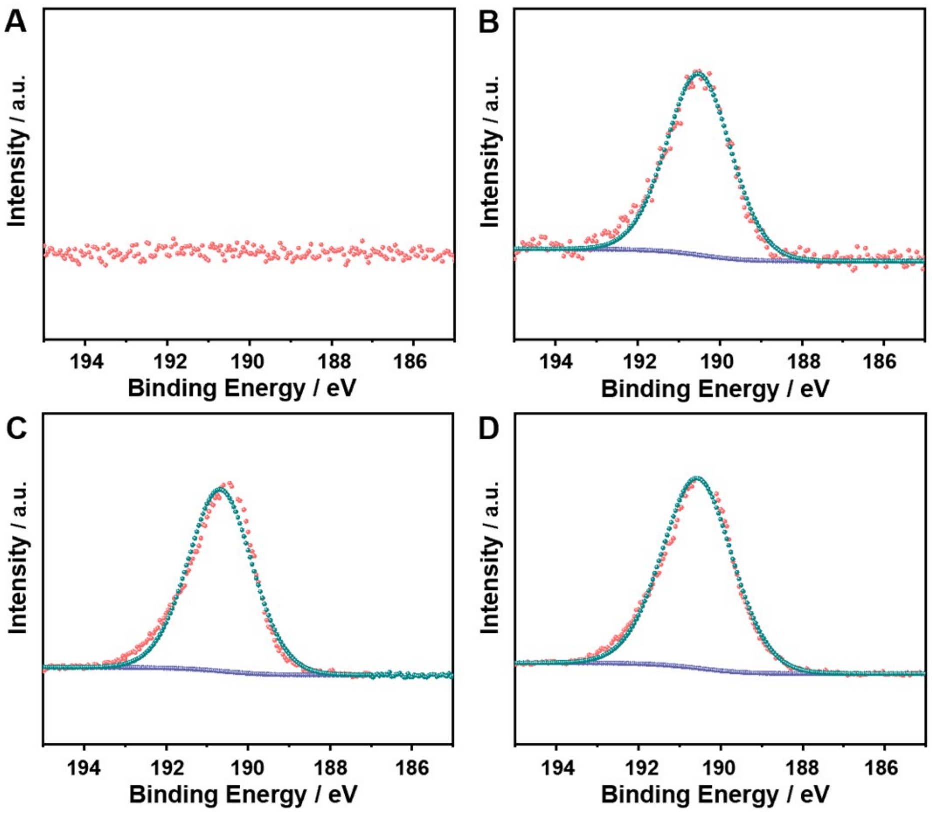

Fig. S9 XPS spectra of B1s orbits for A) Co-N, B) Co-NB-1, C) Co-NB-2, D) Co-NB-3.

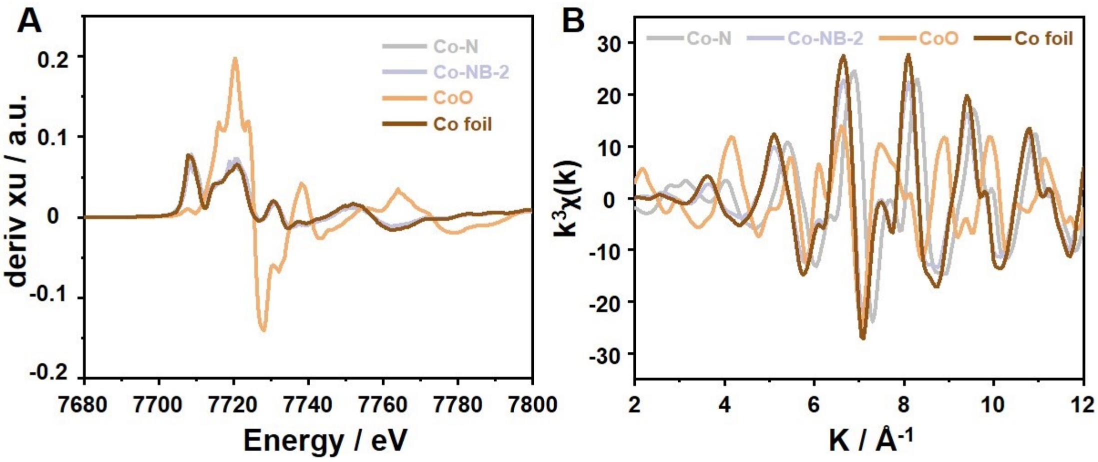

Fig. S10 A) First derivative curves of different samples. B) Co EXAFS spectra of different samples in k space.

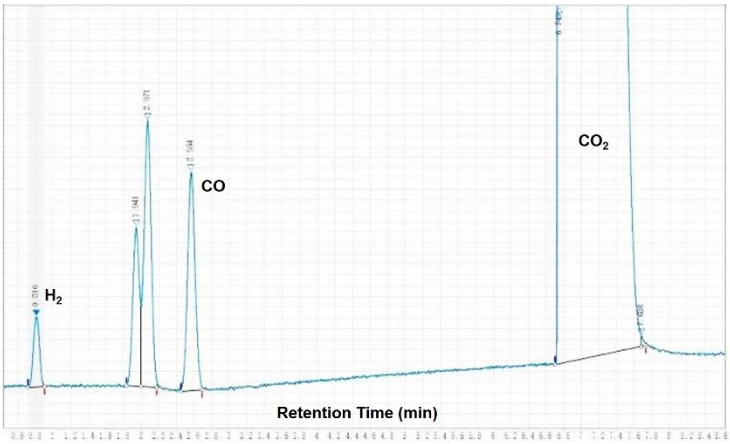

Fig. S11 Gas chromatography of gas products after CO_2 electrolysis on Co-NB-2 at an applied potential of -2.4 V vs Ag/Ag$^+$.

In the presence of only H_2 and CO as products, FE_{CO} can be calculated according to the following equation：

$$FE_{CO} = \frac{12.23A_{CO}}{12.23A_{CO} + A_{H2}}$$

The retention time of 0.810 min corresponds to H_2 with a peak area (A_{H2}) of 13.103 and the retention time of 2.564 min corresponds to CO with a peak area (A_{CO}) of 41.015. FE_{CO} of Co-NB-2 at -2.4 V:

$$FE_{CO} = \frac{12.23 \times 41.015}{12.23 \times 41.015 + 13.103} \times 100\% = 97.5\%$$

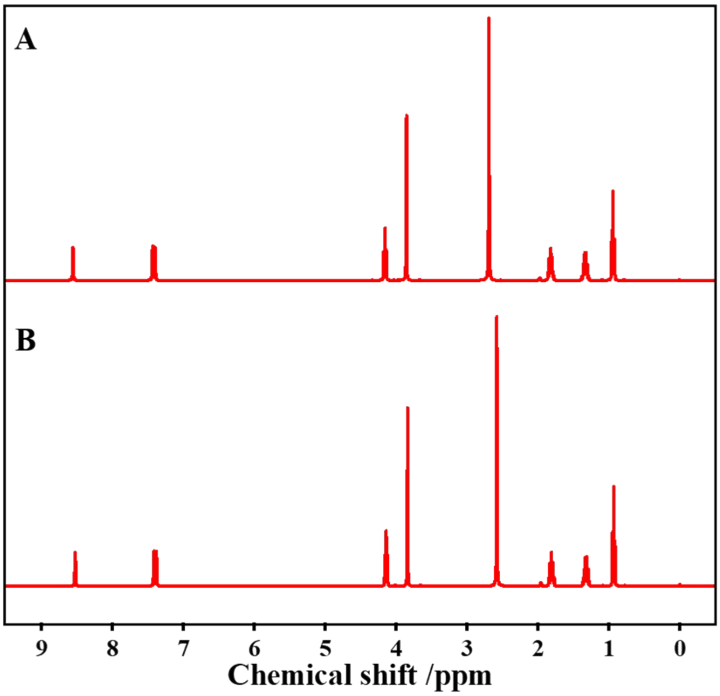

Fig. S12 ^{1}H-NMR spectra of 0.5 M [Bmim]PF$_6$/MeCN before A) and after B) CO$_2$ electrolysis on Co-NB-2 at an applied potential of -2.4 V vs Ag/Ag$^+$ (DMSO-d$_6$).

Based on the ^{1}H NMR spectrum of [Bmim]PF$_6$/MeCN catholyte after 24 h electrolysis over Co-NB-2 at an applied potential of -2.4 V vs. Ag/Ag$^+$ (Fig. S12), we can find that there is no notable change in the spectra, indicating that [Bmim]PF$_6$ was stable during the electrolysis.

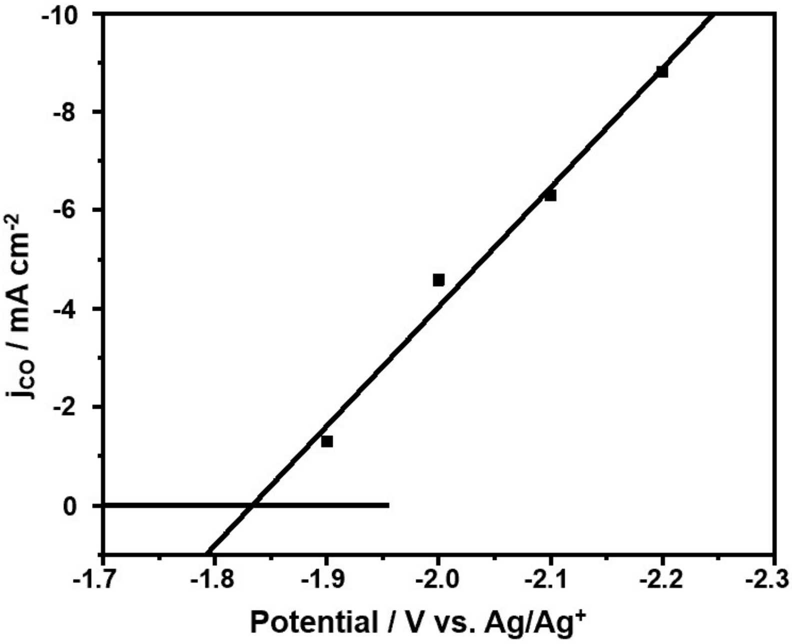

Fig. S13 Current densities for CO production under different potentials and the equilibrium potential obtained by extrapolation method.

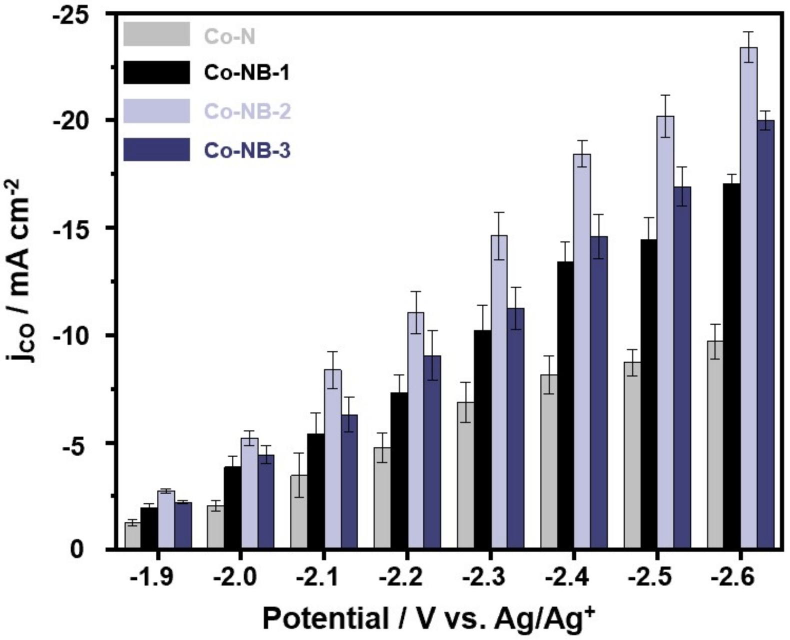

Fig. S14 The partial current density of CO for Co-N, Co-NB-1, Co-NB-2 and Co-NB-3.

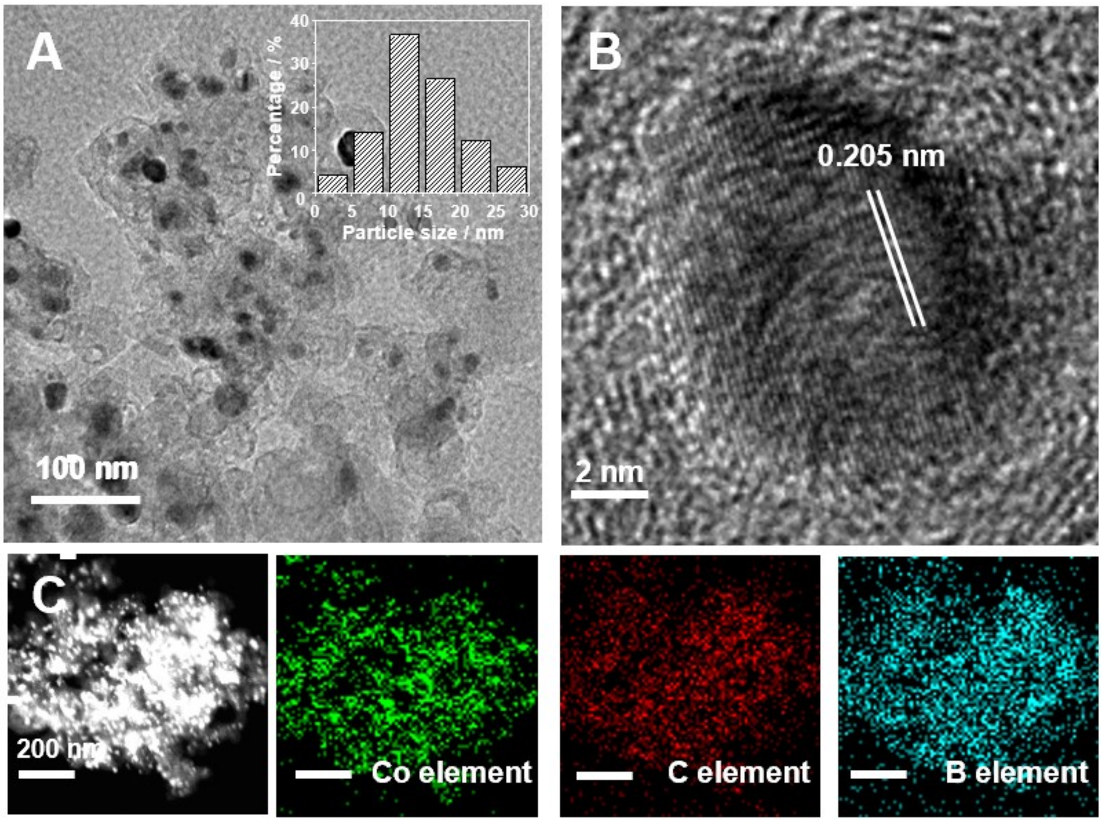

Fig. S15 A) TEM image and particle size distribution, B) HR-TEM image and C) Elemental mappings images of Co-NB-2 after electrolysis.

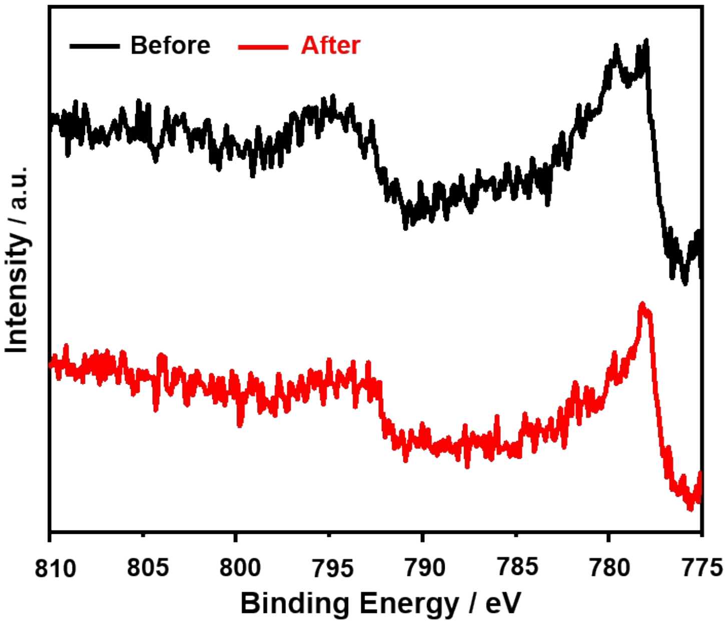

Fig. S16 XPS spectra of Co 2p orbits of Co-NB-2 before and after electrolysis.

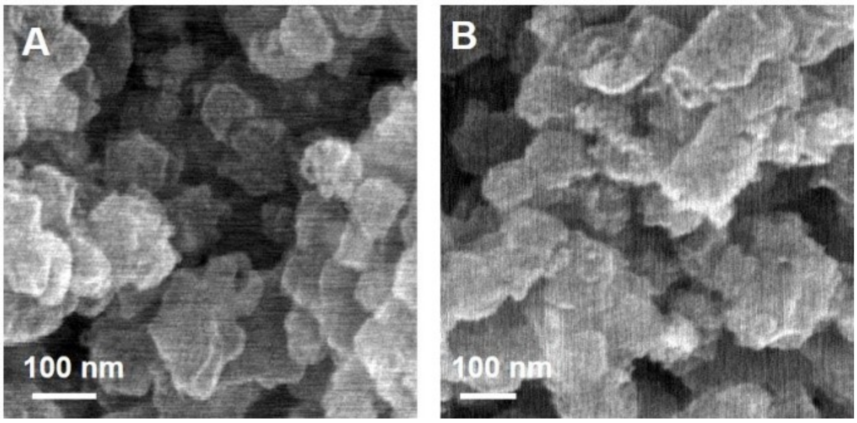

Fig. S17 SEM images of A) Co-NB-1 and B) Co-NB-3 after electrolysis.

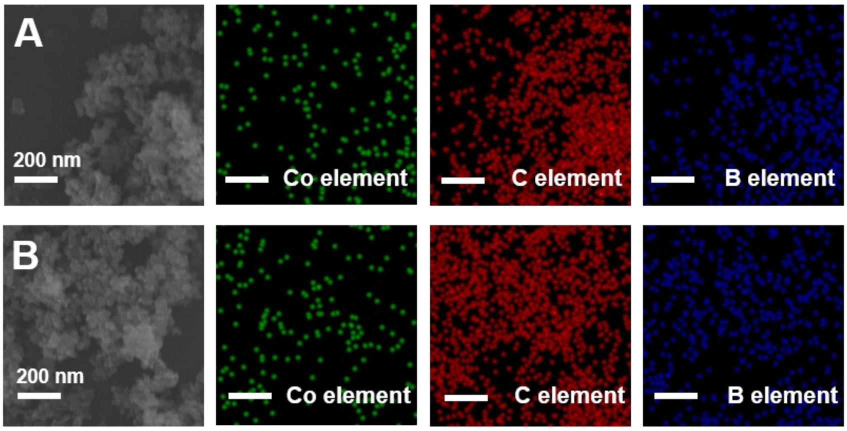

Fig. S18 EDS images of A) Co-NB-1 and B) Co-NB-3 after electrolysis.

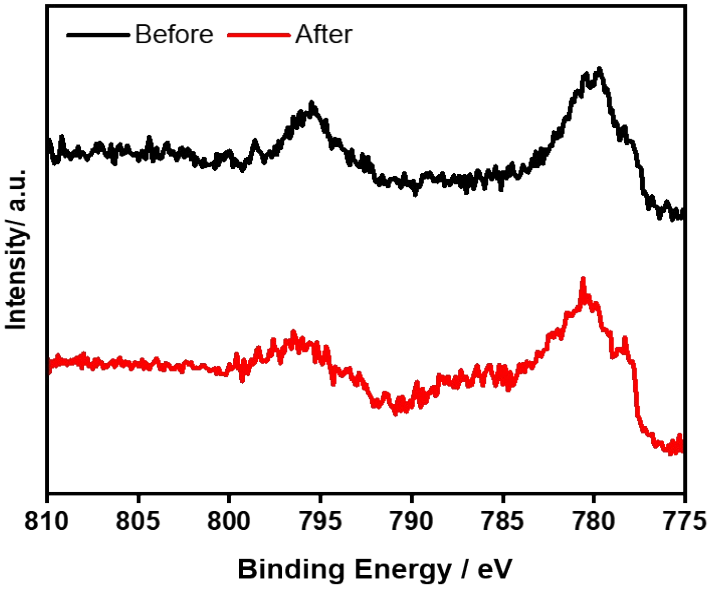

Fig. S19 XPS spectra of Co 2p orbits of Co-NB-1 before and after electrolysis.

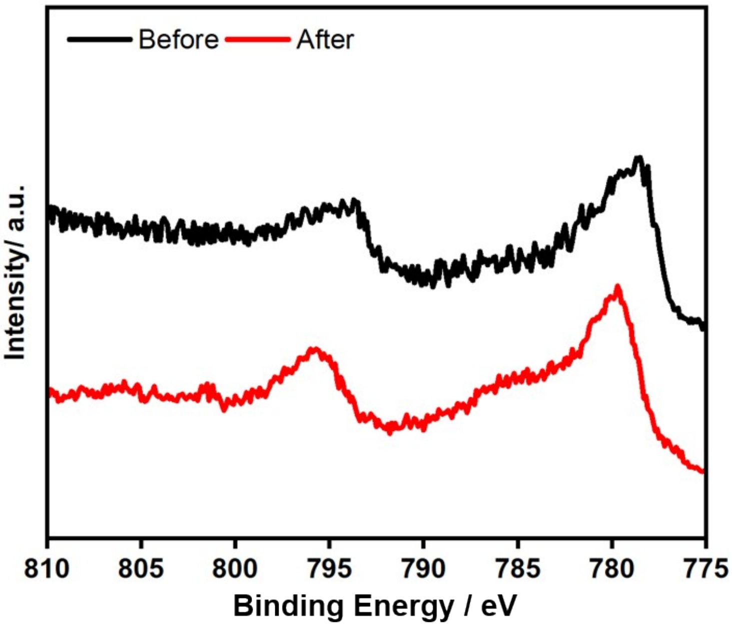

Fig. S20 XPS spectra of Co 2p orbits of Co-NB-3 before and after electrolysis.

Supplementary Tables

Table S1. Comparison of CO_2 reduction performance on different Co-based catalysts.

Electrode	Applied potential /V	Electrolyte	Product, FE/%	Current density / mA cm^{-2}	Ref.
Co-NB-2	-2.4 V vs Ag/Ag^+	0.5 M $[Bmim]PF_6$/ MeCN	CO, 97.9	18.8	This work
$Cu_{50}Co_{50}$ NPs	-1.1 V vs RHE	0.1 M $KHCO_3$	CO, ~2.5	~30	[S2]
Ag-Co bimetallic catalyst	-2.0 V vs SHE	0.5 M $KHCO_3$	CO, 7.8	-	[S3]
Co/Ag(111)	-0.60 V vs. RHE	0.1 M $KHCO_3$	CO, 87	~2	[S4]
Co@CoNC-900	-0.80 V vs. RHE	0.1 M $KHCO_3$	CO, 42	8	[S5]
CoS_2	-0.60 V vs RHE	0.5 M $KHCO_3$	CO, 86	3.3	[S6]
CoPc	-0.70 V vs RHE	1 M $KHCO_3$	CO, 62	3.2	[S7]
CoPc-COF	-0.70 V vs. RHE	0.5 M $KHCO_3$	CO, 93	~10	[S8]
Co-N_2	-0.63 V vs. RHE	0.5 M $KHCO_3$	CO, 94	18.1	[S9]
Co-N_4	-0.48 V vs. RHE	0.1 M $KHCO_3$	CO, 45	~1	[S10]
Co−N_5	-0.79 V vs. RHE	0.2 M $NaHCO_3$	CO, 99.3	10.2	[S11]
CoPc@Zn-N-C	-1.24 V vs. RHE	1 M KOH	CH_4, 18.3	44.3	[S12]
Co_3O_4 layers	-0.87 V vs SCE	0.1 M $KHCO_3$	$HCOO^-$, 85	2.7	[S13]
Ultrathin Co_3O_4	-0.88 V vs SCE	0.1 M $KHCO_3$	$HCOO^-$, 64.3	0.68	[S14]
partially oxidized Co layers	-0.85 V vs SCE	0.1 M Na_2SO_4	$HCOO^-$, 90.1	~10	[S15]
partially oxidized Co particles	-0.90 V vs. SCE	0.1 M $NaHCO_3$	CH_3OH, 71.4	4	[S16]

Table S2. The ICP results of different catalysts.

Sample	Co/wt%
Co-N	6.14
Co-NB-1	14.57
Co-NB-2	11.86
Co-NB-3	9.59

Table S3. The BET results of different catalysts

Sample	S_{BET}/ m^2 g^{-1}
Co-N	584.7
Co-NB-1	410.4
Co-NB-2	137.0
Co-NB-3	29.2

References

S1 D. Gao, H. Zhou, J. Wang, S. Miao, F. Yang, G. Wang, J. Wang and X. Bao, *J. Am. Chem. Soc.*, 2015, **137**, 4288-4291.

S2 M. Bernal, A. Bagger, F. Scholten, I. Sinev, A. Bergmann, M. Ahmadi, J. Rossmeisl and B. R. Cuenya, *Nano Energy*, 2018, **53**, 27-36.

S3 S. Singh, R. K. Gautam, K. Malik and A. Verma, *J. CO_2 Util.*, 2017, **18**, 139-146.

S4 N. Todoroki, H. Tei, T. Miyakawa, H. Tsurumaki and T. Wadayama, *ChemElectroChem*, 2019, **6**, 3101-3107.

S5 R. Daiyan, R. Chen, P. Kumar, N. M. Bedford, J. Qu, J. M. Cairney, X. Lu and R. Amal, *ACS Appl. Mater. Inter.*, 2020, **12**, 9307-9315.

S6 Z. Han, Q. Hu, Z. Cheng, G. Li, X. Huang, Z. Wang, H. Yang, X. Ren, Q. Zhang, J. Liu and C. He, *Adv. Funct. Mater.*, 2020, **30**, 2000154.

S7 B. Hu, W. Xie, R. Li, Z. Pan, S. Song and Y. Wang, *Electrochim. Acta*, 2020, **331**, 135283.

S8 B. Han, X. Ding, B. Yu, H. Wu, W. Zhou, W. Liu, C. Wei, B. Chen, D. Qi, H. Wang, K. Wang, Y. Chen, B. Chen and J. Jiang, *J. Am. Chem. Soc.*, 2021, **143**, 7104-7113.

S9 X. Wang, Z. Chen, X. Zhao, T. Yao, W. Chen, R. You, C. Zhao, G. Wu, J. Wang, W. Huang, J. Yang, X. Hong, S. Wei, Y. Wu and Y. Li, *Angew. Chem. Int. Ed.*, 2018, **57**, 1944-1948.

S10 F. Pan, H. Zhang, K. Liu, D. Cullen, K. More, M. Wang, Z. Feng, G. Wang, G. Wu and Y. Li, *ACS Catal.*, 2018, **8**, 3116-3122.

S11 Y. Pan, R. Lin, Y. Chen, S. Liu, W. Zhu, X. Cao, W. Chen, K. Wu, W.-C. Cheong, Y. Wang, L. Zheng, J. Luo, Y. Lin, Y. Liu, C. Liu, J. Li, Q. Lu, X. Chen, D. Wang, Q. Peng, C. Chen and Y. Li, *J. Am. Chem. Soc.*, 2018, **140**, 4218-4221.

S12 L. Lin, T. Liu, J. Xiao, H. Li, P. Wei, D. Gao, B. Nan, R. Si, G. Wang and X. Bao, *Angew. Chem. Int. Ed.*, 2020, **59**, 22408-22413.

S13 S. Gao, Z. Sun, W. Liu, X. Jiao, X. Zu, Q. Hu, Y. Sun, T. Yao, W. Zhang, S. Wei and Y. Xie, *Nat. Commun.*, 2017, **8**, 14503.

S14 S. Gao, X. Jiao, Z. Sun, W. Zhang, Y. Sun, C. Wang, Q. Hu, X. Zu, F. Yang, S. Yang, L. Liang, J. Wu and Y. Xie, *Angew. Chem. Int. Ed.*, 2016, **55**, 698-702.

S15 S. Gao, Y. Lin, X. Jiao, Y. Sun, Q. Luo, W. Zhang, D. Li, J. Yang and Y. Xie, *Nature*, 2016, **529**, 68-71.

S16 J. Huang, X. Guo, G. Yue, Q. Hu and L. Wang, *ACS Appl. Mater. Inter.*, 2018, **10**, 44403-44414.